

# A Newtonian approach to extraordinarily strong negative refraction

Hosang Yoon<sup>1</sup>, Kitty Y. M. Yeung<sup>1</sup>, Vladimir Umansky<sup>2</sup> & Donhee Ham<sup>1</sup>

Metamaterials with negative refractive indices can manipulate electromagnetic waves in unusual ways, and can be used to achieve, for example, sub-diffraction-limit focusing<sup>1</sup>, the bending of light in the ‘wrong’ direction<sup>2</sup>, and reversed Doppler and Cerenkov effects<sup>2</sup>. These counterintuitive and technologically useful behaviours have spurred considerable efforts to synthesize a broad array of negative-index metamaterials with engineered electric, magnetic or optical properties<sup>1–10</sup>. Here we demonstrate another route to negative refraction by exploiting the inertia of electrons in semiconductor two-dimensional electron gases, collectively accelerated by electromagnetic waves according to Newton’s second law of motion, where this acceleration effect manifests as kinetic inductance<sup>11,12</sup>. Using kinetic inductance to attain negative refraction was theoretically proposed for three-dimensional metallic nanoparticles<sup>13</sup> and seen experimentally with surface plasmons on the surface of a three-dimensional metal<sup>14</sup>. The two-dimensional electron gas that we use at cryogenic temperatures has a larger kinetic inductance than three-dimensional metals, leading to extraordinarily strong negative refraction at gigahertz frequencies, with an index as large as  $-700$ . This pronounced negative refractive index and the corresponding reduction in the effective wavelength opens a path to miniaturization in the science and technology of negative refraction.

The idea of creating negative refraction by exploiting the collective electron acceleration (inertia) effect, or kinetic inductance, was theoretically proposed for specific arrangements of three-dimensional (3D) metallic nanoparticles<sup>13</sup>. Experimentally, inertia-based negative refraction was implied in work where a particular guiding of surface plasmon polaritons on the surface of a 3D metal led to negative refraction<sup>14</sup>; this cannot be explained without electron acceleration, because a defining component of plasmons is the time-varying kinetic energy of their constituent electrons, which implies their acceleration.

Semiconductor two-dimensional (2D) electron gases (2DEGs) possess a much larger kinetic inductance than 3D bulk metals. Here we create negative-index metamaterials by fully exploiting this large kinetic inductance, whose impact is manifested in the extraordinarily large negative index, which we measure to be as large as  $n = -700$ . This is two orders of magnitude larger than the index of  $n \approx -5$  to  $-1$  in surface-plasmon-based negative refraction<sup>14</sup>, and indicates that inertia is a much more important factor in our 2DEG case. It is also much larger than the theoretical expectation based on the kinetic inductance of 3D metallic nanoparticles<sup>13</sup>, which is orders of magnitude smaller than our 2D kinetic inductance (Supplementary Information, section 1).

We choose a GaAs/AlGaAs 2DEG as a demonstration platform. Here electrons can accelerate for  $\sim 0.2$  ns at a temperature of 4 K without scattering, with the result that their large kinetic inductance effect is not masked by the scattering at and above gigahertz frequencies. Specifically, our metamaterial is a periodic array of mesa-etched 2DEG strips (Fig. 1a, b), each of which is connected to ground lines (labelled ‘G’ in Fig. 1a) at both ends via ohmic contacts. Each strip’s width and length are respectively denoted  $W$  and  $l$ , and the centre-to-centre distance between neighbouring strips, or periodicity, is denoted  $a$ .

This metamaterial is excited by electromagnetic waves guided by the left signal line (labelled ‘S’ in Fig. 1a), which, flanked by the ground lines, forms an on-chip coplanar waveguide (CPW) with a  $50\text{-}\Omega$  characteristic impedance. This left signal line is extended to cover a few 2DEG strips on the left-hand side of the metamaterial, with dielectric between the signal line and the 2DEG strips. The metamaterial’s response is picked up by the right signal line (also labelled ‘S’) of another CPW on the right-hand side of the metamaterial.

The electric fields of the excitation electromagnetic wave, oscillating between the signal and ground lines of the left CPW, collectively accelerate electrons in the leftmost few 2DEG strips, producing currents along the strips. The resulting alterations of charge distribution in these strips will capacitively couple to neighbouring strips to the right, accelerating electrons there. This process repeats to deliver an ‘effective wave’ from left to right, perpendicular to the direction of the strips. From the circuit point of view, each 2DEG strip—along which electrons collectively accelerate, with the resulting current lagging the accelerating voltage by  $90^\circ$  according to Newton’s second law of motion—acts as non-magnetic inductance of kinetic origin<sup>11,12</sup>. This 2D kinetic inductance,  $L_{k,2D}$ , results from Newton’s law:  $L_{k,2D} = m^*/(n_{2D}e^2) \times (l_e/W)$ , where  $m^*$ ,  $e$  and  $n_{2D}$  are respectively the electrons’ effective mass, charge and density per unit area, and  $l_e$ , which will be identified shortly, is the effective length of each strip, within which electrons accelerate in response to the excitation. Our metamaterial is then an array of capacitively coupled kinetic inductors (Fig. 1c and Supplementary Information, section 2), and may be

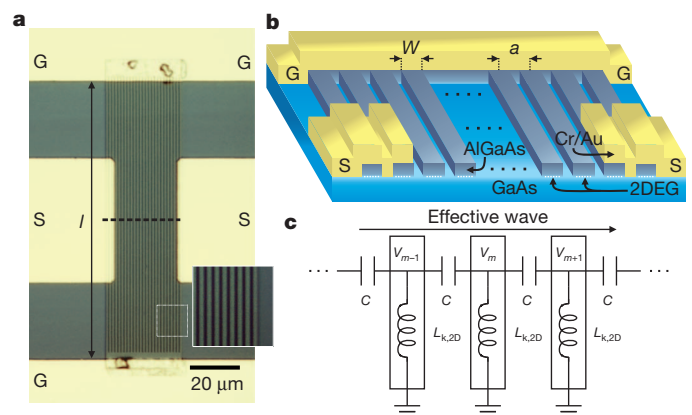


**Figure 1 | Device description.** **a**, Optical image of a 2DEG strip-array metamaterial prototype. Ground-signal-ground (GSG) on-chip CPWs direct electromagnetic waves to and from the metamaterial. The inset shows a magnified portion of the strip array. In this specific prototype,  $W = 1\ \mu\text{m}$ ,  $l = 112\ \mu\text{m}$  and  $a = 1.25\ \mu\text{m}$ . **b**, Schematic of the metamaterial (not drawn to scale), with the front face corresponding to a cut through the dashed symmetry line in **a**. **c**, Circuit description of the half of the metamaterial below or above the symmetry line along the effective wave propagation direction (Supplementary Information, section 2).

<sup>1</sup>School of Engineering and Applied Sciences, Harvard University, Cambridge, Massachusetts 02138, USA. <sup>2</sup>Department of Condensed Matter Physics, Weizmann Institute of Science, Rehovot 76100, Israel.

likened to a left-handed transmission line<sup>15–17</sup>, which is an array of capacitively coupled magnetic inductors and is known to be negatively refracting. However, our negative refraction originates in a different physical phenomenon: our device uses extremely large 2DEG kinetic inductance, whereas the left-handed transmission line relies on a much smaller magnetic inductance.

To examine the negative refraction behaviour of our device, we represent the effective wave, in terms of the voltage at the tip of the  $m$ th kinetic inductor (Fig. 1c), as  $V_m(t) \propto e^{i(\omega t - mka)}$ , where  $\omega$  is the angular frequency and  $k$  is the effective wavenumber. The standard circuit analysis of Fig. 1c yields a dispersion relation  $\omega(k) = \omega_c / |\sin(ka/2)|$ , where  $\omega_c \equiv [2\sqrt{(L_{k,2D}C)}]^{-1}$  is the cut-off frequency at the boundary of the first Brillouin zone ( $k = \pm\pi/a$ ) and  $C$  is the capacitance between adjacent strips over the effective length (Supplementary Information, section 2). For  $\omega > \omega_c$ , the dispersion relation (Fig. 2a) predicts negative refraction, because the tangential slope  $d\omega/dk$  (the group velocity) and the slope  $\omega/k$  (the phase velocity) have opposite signs<sup>10</sup>. The cut-off behaviour results from the metamaterial's high-pass nature, and can also be seen from the current distributions across the metamaterial below and above the cut-off frequency (Fig. 2b), which we simulated using an electromagnetic field solver (Supplementary Information, section 6). Beyond the cut-off frequency (Fig. 2b, right), the current is concentrated at the bottom and top regions of the strips, from which  $l_e$  can be estimated. We note that, whereas a single sheet of 2DEG exhibits ordinary dispersion<sup>18</sup>, the acceleration of electrons along an array of strips of 2DEG, perpendicular to the direction of effective wave propagation, causes negative refraction.

The dispersion relation of our metamaterial has the same form as that of the left-handed transmission line<sup>15–17</sup>, but with the magnetic inductance replaced with the much larger 2DEG kinetic inductance; the 2DEG kinetic inductance is  $1.25 \text{ nH } \mu\text{m}^{-1}$  for a  $1\text{-}\mu\text{m}$  wide 2DEG strip, which is  $\sim 2,800$  times larger than the same strip's magnetic inductance,  $0.44 \text{ pH } \mu\text{m}^{-1}$  (Supplementary Information, section 1). The effective refractive index derived from the dispersion is  $n = -2c/(a\omega) \times \sin^{-1}(\omega_c/\omega)$ , where  $c$  is the speed of light in vacuum, and has the maximum attainable magnitude of  $2c/(a\omega_c) = 4c/a \times \sqrt{(L_{k,2D}C)}$ , which is exceedingly large owing to the large 2DEG kinetic inductance, corresponding to the substantial slowing of the effective wave.

Microwave scattering experiments with on-chip probing confirm this extraordinarily strong negative refraction. The reflection of an electromagnetic wave incident on the left on-chip CPW and its transmission to the right on-chip CPW after propagation through the metamaterial are measured over a range of  $\sim 1\text{--}50$  GHz using a vector

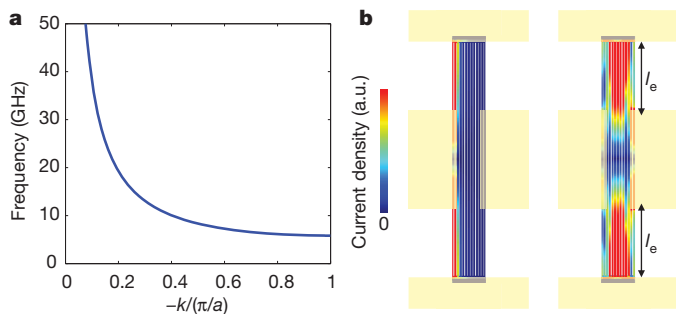


**Figure 2 | Theory and simulation.** **a**, Plot of  $\omega(k) = [2\sqrt{(L_{k,2D}C)}|\sin(ka/2)|]^{-1}$ , with  $L_{k,2D} = 39 \text{ nH}$  and  $C = 4.6 \text{ fF}$  estimated for the structure measured for Fig. 3 ( $W = 1 \mu\text{m}$ ,  $a = 1.25 \mu\text{m}$ ,  $l = 112 \mu\text{m}$ ). The group and phase velocities,  $d\omega/dk$  and  $\omega/k$ , have opposite signs, showing negative refraction; this occurs for both  $k > 0$  and  $k < 0$ , but we show only the latter, which is relevant to our measurements. **b**, Simulated current distributions below (left; 5 GHz) and above (right; 30 GHz) the cut-off frequency. Red and blue colours indicate high and low current densities, respectively. Above the cut-off frequency, regions of high, constant current density are observed, from which the effective strip length  $l_e$  is estimated. a.u., arbitrary units.

network analyser. Propagation delays in the two on-chip CPWs and parasitic couplings between them bypassing the metamaterial were separately measured and de-embedded; from the resulting transmission and reflection coefficients,  $s_{21}$  and  $s_{11}$ , at each measurement frequency, we extract, using a well-established method<sup>19–23</sup>, the effective wave's phasor change  $e^{-ikd}$  due purely to propagation of a distance  $d$  across the metamaterial (Supplementary Information, section 3).

Figure 3a shows the frequency–wavenumber ( $f$ – $k$ ) dispersion so obtained at temperatures of 4.2, 10 and 20 K for a 13-strip metamaterial with  $W = 1 \mu\text{m}$ ,  $l = 112 \mu\text{m}$ ,  $l_e = 31 \mu\text{m}$  and  $a = 1.25 \mu\text{m}$ . Because the measured parameters  $s_{21}$  and  $s_{11}$  set the left-to-right energy propagation direction (that is, the direction of the group velocity) as the positive reference direction, if our metamaterial is negatively refracting, the sign of the extracted wavenumber will be negative with no ambiguity, which is indeed seen in Fig. 3a. Negative refraction is also consistently confirmed in Fig. 3a by the fact that  $d\omega/dk$  and  $\omega/k$  have opposite signs above the 12-GHz cut-off frequency. This measured dispersion, including the cut-off frequency, differs in its details from the calculation that uses lumped circuit elements, ignores losses due to electron scattering in the 2DEG strips and ohmic contacts, and considers only nearest capacitive couplings (Fig. 2). But it has the same underlying features, demonstrating negative refraction. The dark area in Fig. 3a, where the distinctively spurious behaviour of the dispersion appears, is indicative of the cut-off region, which is irrelevant to the operation of the device (Supplementary Information, section 3). From this  $f$ – $k$  dispersion, we obtain the effective refractive index using  $n = kc/\omega$ , whose real part is as large as  $-500$  (Fig. 3b). This large negative index, which is difficult, if not impossible, to achieve with magnetic inductance<sup>3–5,15–17,24,25</sup>, allows drastic device miniaturization and can facilitate ultra-subwavelength localization. The same measurements performed on the 2DEG strip array, but with energy propagation along the strips, yield positive refraction, further highlighting our negative refraction strategy (Supplementary Information, section 5).

We find that  $|\text{Re}(n)|$  decreases with frequency (Fig. 3b), because as the frequency increases adjacent strips are coupled more capacitively, which increasingly bypasses the electron acceleration effect within each separated strip. Figure 3c shows the figure of merit,  $|\text{Re}(n)/\text{Im}(n)|$ , which here reflects losses due to electron scattering in the 2DEG strips and ohmic contacts. It takes a value of  $\sim 2$  over a reasonably large part of the negative refraction region, similarly to negative refraction devices using metals at optical frequencies<sup>24,25</sup>. Figure 3a–c shows that the negative refraction behaviour is essentially the same regardless of temperature (4.2, 10 and 20 K), indicating that the degree of electron scattering in the 2DEG strips and ohmic contacts remains largely the same within this temperature range, not masking the inertia effect. In Fig. 3c, the figure of merit is largest at 10 K instead of at 4.2 K, but these variations with respect to temperature arise mostly from inconsistent probe landings during multiple calibration steps, which are done for measurements at each temperature. Fluctuations at high frequencies, for example, in Fig. 3c, are also due to imperfect calibration.

At 297 K, electron scattering in each 2DEG strip becomes so severe that the acceleration effect is completely masked. Equivalently, the strip's ohmic resistance becomes far larger ( $\sim 100 \text{ k}\Omega$ ) than the impedance of its kinetic inductance. The strip array then becomes essentially an open circuit, causing the signal to be mostly reflected. This reflection can be seen from the value of the reflection coefficient,  $|s_{11}| \approx 1$ , measured at 297 K, which differs from  $|s_{11}|$  at cryogenic temperatures, where the strip array exhibits negative refraction (Fig. 3d). The transmission coefficient,  $|s_{21}|$ , becomes smaller at 297 K also because of the open-circuit behaviour, but is not unappreciable (Fig. 3d). To understand this, we fabricated exactly the same structure as the previous device, but without the strip array, thus creating an actual open circuit between the two on-chip CPWs. The behaviour of  $|s_{21}|$  for this open device at 4.2 K closely resembles that of  $|s_{21}|$  for the strip array at 297 K (Fig. 3d). This demonstrates that the behaviour in the strip array at 297 K is due largely to the parasitic coupling between the two CPWs bypassing the

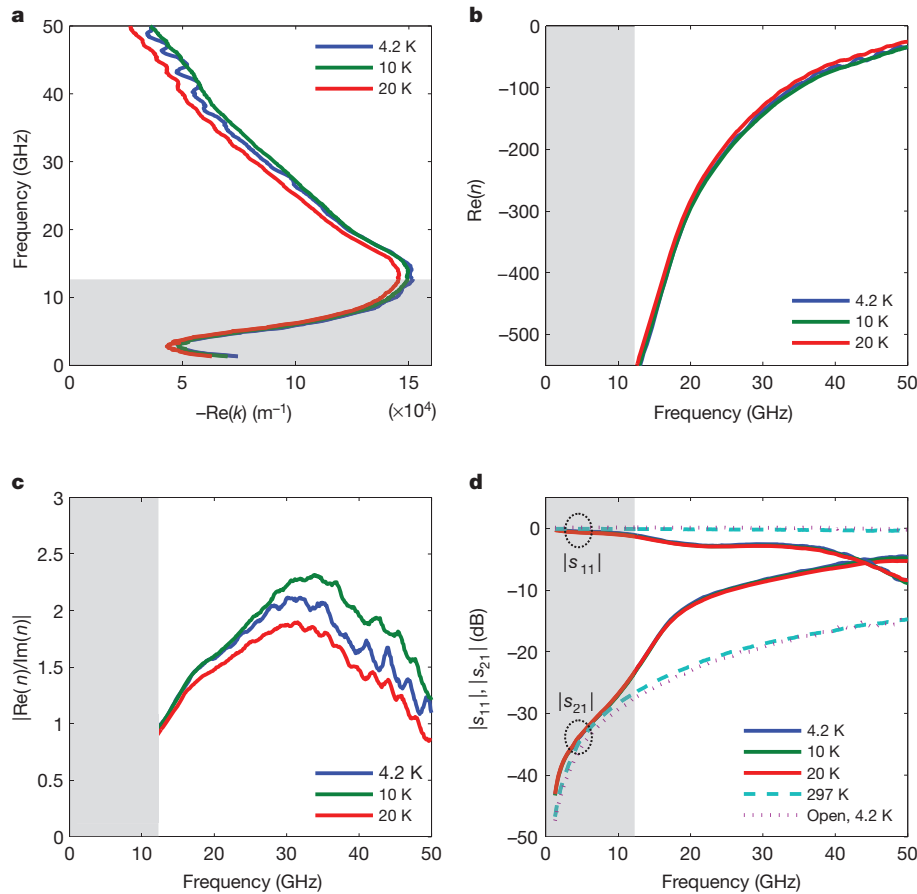


**Figure 3 | Temperature-dependent measurements.** **a**, Dispersion of the 13-strip metamaterial at 4.2, 10, and 20 K. The dark region is indicative of the cut-off behaviour. **b**,  $\text{Re}(n)$  versus frequency. **c**, Figure of merit  $|\text{Re}(n)/\text{Im}(n)|$  versus frequency. **d**, Parameters  $|s_{11}|$  and  $|s_{21}|$  of the metamaterial, separately

strip array, confirming the open-circuit nature of the device at 297 K (in fact, the phases of the transmission and reflection parameters are also much the same in the open device at 4.2 K and the strip array at 297 K; see Supplementary Information, section 4). These results provide further confirmation that the negative refraction we observe at cryogenic temperatures is due to the kinetic inductance. Also, in most of the dark area in Fig. 3d, the  $|s_{21}|$  value of the metamaterial even at cryogenic temperatures is very similar to that of the open device, confirming the cut-off nature in that region.

To examine further the impact of kinetic inductance on negative refraction, we measure a new set of devices of various geometric parameters. Comparison of devices with different values of  $l$  (and, thus,  $l_e$ ) for the same values of  $W$  and  $a$  is especially instructive; changing  $l$  scales  $L_{k,2D}$ ,  $C$  and  $\omega_c$  proportionally to  $l_e$ , affecting the index  $n = -(2c/a\omega) \times \sin^{-1}(\omega_c/\omega)$  with only one parameter,  $\omega_c$ . Specifically, a device with longer strips, with larger values of  $L_{k,2D}$  and  $C$ , and a smaller  $\omega_c$  value, will have a negative index with a larger maximum attainable magnitude,  $2c/a\omega_c$ , reaching the frequency region forbidden for a shorter-strip device. In the frequency region accessible by both longer- and shorter-strip devices, the shorter-strip device will have a larger negative index than the longer-strip device if the two are compared at the same frequency (Supplementary Fig. 4). This clear-cut property emerges in measurements of a pair of devices both with  $a = 1.25 \mu\text{m}$  but with differing values of  $l$  (112 versus  $52 \mu\text{m}$ ) or  $l_e$  (31 versus  $14 \mu\text{m}$ ) (Fig. 4a). This property is confirmed again in two additional pairs of devices (Fig. 4b), where the refractive index is as large as  $-700$ .

Altering the periodicity  $a$ , which in general may have to be combined with altering  $W$ , affects the index  $n = -(2c/a\omega) \times \sin^{-1}(\omega_c/\omega)$

indicated by the dashed ovals, at 4.2, 10, 20 and 297 K. Also shown are  $|s_{11}|$  and  $|s_{21}|$  of the open-circuit device at 4.2 K. Unlike the data in **a**, **b** and **c**, these are 'raw'  $s$  parameters without de-embedding, showing the parasitic coupling between the two CPWs.

in a more complicated manner, owing to simultaneous changes in  $a$  and  $\omega_c$ . For  $l = 112 \mu\text{m}$ , as we decrease  $(a, W)$  first from  $(1.5 \mu\text{m}, 1 \mu\text{m})$  to  $(1.25 \mu\text{m}, 1 \mu\text{m})$  and then to  $(0.75 \mu\text{m}, 0.6 \mu\text{m})$ , with the first reduction increasing  $C$  by a factor of 1.2 with  $L_{k,2D}$  unchanged, and the second reduction increasing  $L_{k,2D}$  by a factor of 1.7 with  $C$  unchanged,  $\omega_c$  does not vary as much as  $a$ , owing to the square-root dependence of  $\omega_c$  on  $L_{k,2D}$  and  $C$ . Thus, a smaller periodicity will yield a larger negative index for the same frequency away from the cut-off regions, as evident in measurements (Fig. 4c). In these  $a$  and  $W$  variations, the characteristic impedance and, thus, the impedance mismatch is varied. This results in imperfect de-embedding of the parasitic couplings near cut-offs, obscuring the cut-off behaviours. The tendency of the index to be more negative for smaller periodicities is seen again for  $l = 52 \mu\text{m}$  with the same variations of  $a$  and  $W$  (Fig. 4d). The crossing of the respective data for the devices with  $a = 1.25$  and  $1.5 \mu\text{m}$  is an anomaly that we suspect arises from the impedance mismatch variation.

The exceedingly strong inertia-based negative refraction demonstrated here requires a solid-state platform with a very large kinetic inductance and low electron scattering. To meet these requirements, we used a GaAs/AlGaAs 2DEG at cryogenic temperature. Scaling the 2DEG metamaterial to higher frequencies by simultaneous reduction of the strip length and periodicity (Fig. 4 and Supplementary Information, section 2) would relax the condition on electron scattering time (and, thus, temperature); demonstration<sup>26</sup> of terahertz plasmonic devices at room temperature with GaAs/AlGaAs 2DEG bodes well for high-temperature applications. Graphene, another type of 2D conductor with high mobility at room temperature<sup>27</sup>, may also be a platform for terahertz-frequency negative refraction based on a

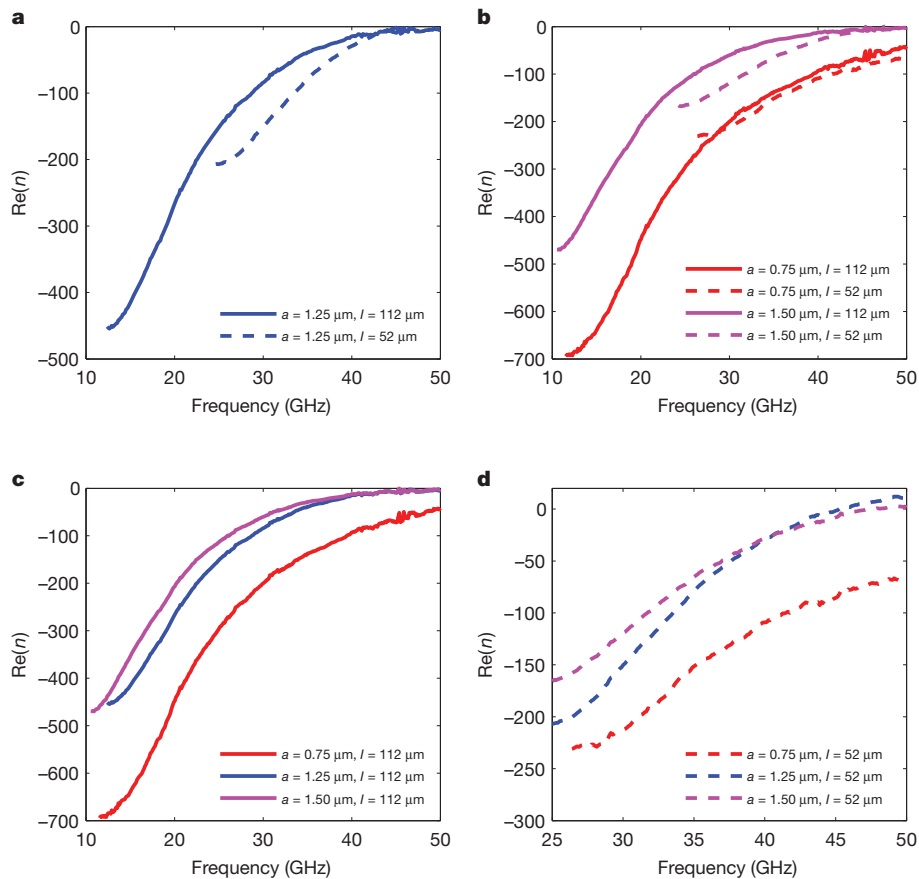


**Figure 4 | Geometry-dependent measurements at 4.2 K.** **a**,  $\text{Re}(n)$  for a pair of 13-strip metamaterials with  $a = 1.25 \mu\text{m}$  and  $W = 1 \mu\text{m}$ , but with different  $l$  values. **b**,  $\text{Re}(n)$  for another two pairs of 13-strip metamaterials with different  $l$  values:  $(a, W) = (0.75 \mu\text{m}, 0.6 \mu\text{m})$  and  $(1.50 \mu\text{m}, 1 \mu\text{m})$ . **c**,  $\text{Re}(n)$  for  $l = 112 \mu\text{m}$

similar kinetic approach. Although electrons in graphene act as massless particles, and thus are non-Newtonian, they still possess kinetic energy, exhibiting plasmonic behaviour with implicit kinetic inductance. In fact, terahertz light–plasmon coupling has been recently observed at room temperature<sup>28</sup>. Achieving strong negative refraction based on the kinetic approach with higher isotropy and at optical frequencies using different material systems is also open to further investigation.

## METHODS SUMMARY

We fabricate the devices on GaAs/AlGaAs 2DEG substrates obtained by molecular beam epitaxy. The layer structure above the 2DEG comprises 40-nm  $\text{Al}_{0.36}\text{Ga}_{0.64}\text{As}$ , 14-nm Si-doped  $\text{Al}_{0.36}\text{Ga}_{0.64}\text{As}$ , 10-nm  $\text{Al}_{0.36}\text{Ga}_{0.64}\text{As}$  and a 7-nm GaAs cap. At 4 K, the mobility of the 2DEG is  $4.6 \times 10^6 \text{ cm}^2 \text{ V}^{-1} \text{ s}^{-1}$  and the carrier density is  $1.9 \times 10^{11} \text{ cm}^{-2}$ , both in the dark. 2DEG strips are defined by electron beam lithography, followed by wet etching (>71-nm depth) with 150:1:1  $\text{H}_2\text{O}:\text{H}_2\text{O}_2:\text{NH}_4\text{OH}$ . Ohmic contacts are defined by photolithography followed by thermal evaporation of Ni (5 nm)/Au (20 nm)/Ge (25 nm)/Au (10 nm)/Ni (5 nm)/Au (40 nm), and annealing at 420 °C for 50 s. CPWs are defined by photolithography and formed by thermal evaporation of Cr (8 nm)/Au (500 nm).

The microwave scattering analysis is performed in a Lake Shore Cryotronics cryogenic probe station at feedback-controlled cryogenic temperatures in the dark. Ground–signal–ground microwave probes, with a pitch of 100  $\mu\text{m}$ , connected to probe arms are attached to on-chip CPWs. Coaxial cables lead to the probes from an Agilent E8364A network analyser, which generates excitation signals of frequencies up to 50 GHz, delivering  $-45 \text{ dBm}$  power to the devices, and measures the scattering parameters. To see the effect of the metamaterial (strip array) only, we first calibrate the system, at each measurement temperature, up to the tips of the probes by using the NIST-style multiline TRL technique<sup>29</sup>, and then perform additional de-embedding to remove the on-chip CPW delays and parasitic couplings between the CPWs, which bypass the metamaterial (Supplementary Information, section 3). The CPWs used for this calibration<sup>30</sup> are fabricated on

undoped GaAs substrates and designed using a Sonnet electromagnetic solver to have a 50- $\Omega$  characteristic impedance, which is the characteristic impedance of the network analyser, cables and probes.

Received 2 December 2011; accepted 31 May 2012.

Published online 1 August 2012.

- Pendry, J. B. Negative refraction makes a perfect lens. *Phys. Rev. Lett.* **85**, 3966–3969 (2000).
- Veselago, V. G. The electrodynamics of substances with simultaneously negative values of  $\epsilon$  and  $\mu$ . *Sov. Phys. Usp.* **10**, 509–514 (1968).
- Smith, D. R., Padilla, W. J., Vier, D. C., Nemat-Nasser, S. C. & Schultz, S. Composite medium with simultaneously negative permeability and permittivity. *Phys. Rev. Lett.* **84**, 4184–4187 (2000).
- Shelby, R. A., Smith, D. R. & Schultz, S. Experimental verification of a negative index of refraction. *Science* **292**, 77–79 (2001).
- Linden, S. *et al.* Photonic metamaterials: magnetism at optical frequencies. *IEEE J. Sel. Top. Quantum Electron.* **12**, 1097–1105 (2006).
- Cubukcu, E., Aydin, K., Ozbay, E., Foteinopoulou, S. & Soukoulis, C. M. Electromagnetic waves: negative refraction by photonic crystals. *Nature* **423**, 604–605 (2003).
- Valentine, J. *et al.* Three-dimensional optical metamaterial with a negative refractive index. *Nature* **455**, 376–379 (2008).
- Podolskiy, V. A. & Narimanov, E. E. Strongly anisotropic waveguide as a nonmagnetic left-handed system. *Phys. Rev. B* **71**, 201101 (2005).
- Hoffman, A. J. *et al.* Negative refraction in semiconductor metamaterials. *Nature Mater.* **6**, 946–950 (2007).
- Pendry, J. B. A chiral route to negative refraction. *Science* **306**, 1353–1355 (2004).
- Meservey, R. Measurements of the kinetic inductance of superconducting linear structures. *J. Appl. Phys.* **40**, 2028–2034 (1969).
- Burke, P. J., Spielman, I. B., Eisenstein, J. P., Pfeiffer, L. N. & West, K. W. High frequency conductivity of the high-mobility two-dimensional electron gas. *Appl. Phys. Lett.* **76**, 745–747 (2000).
- Engheta, N. Circuits with light at nanoscales: optical nanocircuits inspired by metamaterials. *Science* **317**, 1698–1702 (2007).
- Lezec, H. J., Dionne, J. A. & Atwater, H. A. Negative refraction at visible frequencies. *Science* **316**, 430–432 (2007).

15. Eleftheriades, G. V., Iyer, A. K. & Kremer, P. C. Planar negative refractive index media using periodically L-C loaded transmission lines. *IEEE Trans. Microw. Theory Tech.* **50**, 2702–2712 (2002).
16. Caloz, C. & Itoh, T. Transmission line approach of left-handed (LH) materials and microstrip implementation of an artificial LH transmission line. *IEEE Trans. Antenn. Propag.* **52**, 1159–1166 (2004).
17. Grbic, A. & Eleftheriades, G. V. Overcoming the diffraction limit with a planar left-handed transmission-line lens. *Phys. Rev. Lett.* **92**, 117403 (2004).
18. Stern, F. Polarizability of a two-dimensional electron gas. *Phys. Rev. Lett.* **18**, 546–548 (1967).
19. Chen, X., Grzegorzczak, T. M., Wu, B.-I., Pacheco, J. & Kong, J. A. Robust method to retrieve the constitutive effective parameters of metamaterials. *Phys. Rev. E* **70**, 016608 (2004).
20. Smith, D. R., Vier, D. C., Koschny, T. & Soukoulis, C. M. Electromagnetic parameter retrieval from inhomogeneous metamaterials. *Phys. Rev. E* **71**, 036617 (2005).
21. Burgos, S. P., de Waele, R., Polman, A. & Atwater, H. A. A single-layer wide-angle negative-index metamaterial at visible frequencies. *Nature Mater.* **9**, 407–412 (2010).
22. Choi, M. *et al.* A terahertz metamaterial with unnaturally high refractive index. *Nature* **470**, 369–373 (2011).
23. Chanda, D. *et al.* Large-area flexible 3D optical negative index metamaterial formed by nanotransfer printing. *Nature Nanotechnol.* **6**, 402–407 (2011).
24. Shalaev, V. M. Optical negative-index metamaterials. *Nature Photon.* **1**, 41–48 (2007).
25. Soukoulis, C. M., Linden, S. & Wegener, M. Negative refractive index at optical wavelengths. *Science* **315**, 47–49 (2007).
26. Meziani, Y. M. *et al.* Room temperature terahertz emission from grating coupled two-dimensional plasmons. *Appl. Phys. Lett.* **92**, 201108 (2008).
27. Dean, C. R. *et al.* Boron nitride substrates for high-quality graphene electronics. *Nature Nanotechnol.* **5**, 722–726 (2010).
28. Ju, L. *et al.* Graphene plasmonics for tunable terahertz metamaterials. *Nature Nanotechnol.* **6**, 630–634 (2011).
29. Marks, R. B. A multilayer method of network analyzer calibration. *IEEE Trans. Microw. Theory Tech.* **39**, 1205–1215 (1991).
30. Andress, W. F. *et al.* Ultra-subwavelength two-dimensional plasmonic circuits. *Nano Lett.* **12**, 2272–2277 (2012).

**Supplementary Information** is linked to the online version of the paper at [www.nature.com/nature](http://www.nature.com/nature).

**Acknowledgements** The authors are grateful for support for this research by the Air Force Office of Scientific Research under contract numbers FA 9550-09-1-0369 and FA 9550-08-1-0254. Device fabrication was performed in part at the Center for Nanoscale Systems at Harvard University. The authors thank W. F. Andress for assistance with device fabrication and microwave measurements.

**Author Contributions** H.Y. and D.H. had the idea for the project. V.U. fabricated the 2DEG. H.Y. designed, fabricated and measured the properties of the devices. H.Y., K.Y.M.Y. and D.H. analysed the data. H.Y. and D.H. wrote the paper. All authors discussed the results and reviewed the manuscript.

**Author Information** Reprints and permissions information is available at [www.nature.com/reprints](http://www.nature.com/reprints). The authors declare no competing financial interests. Readers are welcome to comment on the online version of this article at [www.nature.com/nature](http://www.nature.com/nature). Correspondence and requests for materials should be addressed to D.H. ([donhee@seas.harvard.edu](mailto:donhee@seas.harvard.edu)).